TECHNICAL PAPER

Multiple model-based fault-tolerant control system for distributed drive electric vehicle

Liangjiang Liu[1] · Ke Shi[2] · Xiaofang Yuan[2] · Qingxian Li[1]

Abstract

Generally, the distributed drive electric vehicle (DDEV) works under different fault status, and this may lead to unstable operating performance. However, the conventional fault-tolerant controller is only suitable for one special fault status, and thus, the stability of DDEV is hard to be guaranteed efficiently. To deal with this problem, a novel multiple model-based fault-tolerant control system (MMFTCS) is proposed in this paper. The MMFTCS integrates an operating status recognizer and a fault-tolerant controller set. The operating status recognizer is designed to distinguish current operating status, where the matching degree between current operating status and typical operating mode set is detected using fuzzy logic. The fault-tolerant controller set is designed to achieve optimal fault-tolerant control, and each fault-tolerant controller is designed for the corresponding typical operating mode by the model predictive controller. The output of the MMFTCS is computed by the weighted signal of each fault-tolerant controller to realize smooth switching. The simulation is carried on the MATLAB environment, and the results show that the MMFTCS has excellent fault-tolerant performance under various operating status.

1 Introduction

Compared with a traditional vehicle, the main advantage of distributed drive electric vehicle (DDEV) is that more actuators can be controlled, and this advantage provides a possibility to achieve better stability performance [1, 2]. In the past few decades, the studies of vehicle stability have become an active area in the automotive field [3]. However,

✉ Liangjiang Liu
  41326337@qq.com

  Ke Shi
  samkieth@hnu.edu.cn

  Xiaofang Yuan
  yuanxiaofang@hnu.edu.cn

  Qingxian Li
  lqxpc@163.com

[1] Hunan Institute of Metrology and Test, Changsha, Hunan, China

[2] College of Electrical and Information Engineering, Hunan University, Changsha, Hunan, China

the stability performance of DDEV is usually affected by the unknown fault, especially the actuator fault [4, 5].

In general, the actuator fault occurring on the steering system or in-wheel motor may result in unwanted effect and jeopardize of the vehicle motion [6, 7]. When a fault occurs on the in-wheel motor or steering system, the faulty wheel or faulty steering system may fail to provide the expected torque or expected steering angle, respectively [8, 9]. In these cases, the difficulty of stability control of DDEV is increased. Therefore, the fault-tolerant controller has been proposed to overcome the effect of fault in the actuator of vehicle [10, 11]. In detail, the actuator fault type is usually divided into loss-of-effectiveness actuator fault and struck at a fixed-level actuator fault [12]. Dual-motor controller control system architectures for loss-of-effectiveness actuator fault is adopted [13]. Aiming to reduce the struck at a fixed-level actuator fault, analytical redundancy-based methods are proposed [14].

For the fault-tolerant method, many control algorithms have been designed. The sliding mode controllers are designed to solve the problems of longitudinal velocity, lateral velocity and yaw rate, respectively [15]. The structural recoverability algorithm has been proposed to solve the

redundancy actuator fault efficiently [16]. As an efficient method, the adaptive control is designed for active fault diagnosis [17]. For solving the actuator fault with external disturbance and parameter uncertainty, the robustness H ∞ controller has been utilized [18]. However, most of the above-mentioned fault-tolerant controllers are only designed for one special fault status. Therefore, the stability of DDEV under various fault status is difficult to be guaranteed.

To solve the various fault status problem, a novel MMFTCS is proposed. The MMFTCS integrates an operating status recognizer and a fault-tolerant controller set, and both of two parts are designed based on multiple model method. The main merits of this work cover the following points:

(1) To classify the different fault status, the operating status of DDEV can be divided into eight typical operating modes, including a normal mode and seven fault modes.

(2) To distinguish current status accurately, the matching degree between current operating status and typical operating mode set is represented as the weight coefficient, in the operating status recognizer.

(3) The fault-tolerant controller set is designed for each typical operating mode to deal with the different actuator faults problem, and realized by the linear-quadratic regulation-based model predictive controller (LQR-MPC).

(4) To guarantee the practicability to each typical operating mode and to realize smooth switching, the weighted outputs of the fault-tolerant controller constitute the control output of MMFTCS.

The organization of this paper is presented. In Sect. 2, the system model is built and the control problems are stated. In Sect. 3, both the implementation and the robustness analysis of MMFTCS are presented. Section 4 gives the simulation results to validate the performance of MMFTCS. Finally, the conclusions are summarized in Sect. 5.

2 System modelling and steering performance analysis

In this section, the vehicle, tyre and actuator fault models are established, respectively. The symbols and definitions of DDEV are listed in Table 1.

2.1 Vehicle model with various actuators

The vehicle model with various actuators is established based on two-degree-of-freedom (2DOF) plane as shown in

Table 1 Symbols of vehicle model

Definition	Symbol	Value	Unit
Vehicle sideslip angle	β	–	rad
Vehicle yaw rate	γ	–	rad/s
Vehicle yaw moment	M_z	–	Nm
Vehicle mass	m	1359.8	kg
Vehicle yaw moment of inertia	I_z	1992.54	kgm^2
Distance from c.g. to front axle	l_f	1.0628	m
Distance from c.g. to rear axle	l_r	1.4852	m
Longitudinal stiffness of four tyres	$C_{ki}, i = fl, fr, rl, rr$	–	N/rad
Front cornering stiffness	C_f	23540	N/rad
Rear cornering stiffness	C_r	23101	N/rad
Tyre radius	r	0.29	m
Sideslip angle of front and rear tyres	α_f, α_r	–	rad
Front steering angle from driver/controller	δ, δ_f	–	rad
Longitudinal force of four tyres	$F_{xi}, i = fl, fr, rl, rr$	–	N
Later force of four tyres	$F_{yi}, i = fl, fr, rl, rr$	–	N
Moment of inertia of each tyre	J	0.3534	kgm^2
Friction coefficient of road	μ	0.6	-
Total drive torque	T_t	–	Nm
In-wheel motor torques	$T_i, i = fl, fr, rl, rr$	–	Nm
Fitting coefficients	K_a, K_b	–	-
Vehicle velocity	v	–	km/h
Vehicle longitudinal velocity	v_x	–	km/h

Fig. 1 [19]. The coupling problems of longitudinal, lateral and vertical dynamic are ignored.

$$\dot{\beta} = \frac{F_{yf} + F_{yr}}{mv} - \gamma \tag{1}$$

$$\dot{\gamma} = \frac{F_{yf} \cdot l_f - F_{yr} \cdot l_r + M_z}{I_z} \tag{2}$$

where $M_z = \frac{l_f + l_r}{2}(-F_{xfl} + F_{xfr} - F_{xrl} + F_{xrr})$.

2.2 Tyre model with various actuators

The tyre model with various actuators is formulated based on the magic model, which integrates the driving system and steering system [20].

$$F_i = \Gamma \sin(\Omega \arctan(X - Y(\Phi X - \arctan(\Phi X)))) \tag{3}$$

where Φ, Ω, Γ and Y are the stiffness, shape, peak and curvature factors, respectively. X is the input variable of tyre model.

2.2.1 Driving system

In general, F_x is formulated as a linear approximation according to the magic model (3). The expression of F_x can be simplified as (4):

$$F_{xi} = C_{ki} \cdot \kappa_i, i = fl, fr, rl, rr \tag{4}$$

where $C_{ki} = F_{zi} \cdot (p_{Kx1} + p_{Kx2} \cdot df_z) \cdot \exp(p_{Kx3} \cdot df_z)$. p_{Kx1}, p_{Kx2} and p_{Kx3} are fitting coefficients. F_z is the tyre vertical load.

To calculate the required motor torque, a torque balance equation is formed for each tyre without considering the vehicle vertical load transfer [21]. Therefore, F_x of a single tyre is calculated as $F_x = \frac{1}{4}m\dot{v}$, and the relationship between κ and T is expressed as:

$$\dot{\kappa}_i = \left(\frac{4 \cdot (\kappa_i + 1)}{m \cdot v} + \frac{(\kappa_i + 1)^2 \cdot r^2}{J \cdot v} \right) \cdot C_{ki} - \frac{(\kappa_i + 1)^2 \cdot r \cdot T_i}{J \cdot v} \tag{5}$$
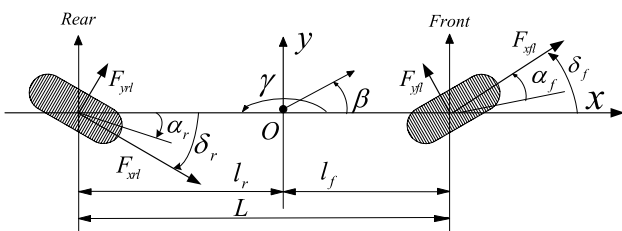

Fig. 1 The 2DOF vehicle model

2.2.2 Steering system

Here, F_{yf} and F_{yr} are linear functions of α_f and α_r [21], respectively. After linear approximation, the expression for F_y can be simplified as (6):

$$F_{yj} = C_j \cdot \alpha_j, j = f, r \tag{6}$$

By assuming that v_x is equal to v, then,

$$\dot{\alpha}_f = \frac{F_{yf} + F_{yr}}{mv} - \frac{v}{l_f + l_r} \cdot (\alpha_f - \alpha_r - \delta_f + \delta_r)$$
$$+ \frac{l_f}{vI_z} \cdot (l_f F_{yf} - l_r F_{yr} + M_z) - \dot{\delta}_f \tag{7}$$

$$\dot{\alpha}_r = \frac{F_{yf} + F_{yr}}{mv} - \frac{v}{l_f + l_r} \cdot (\alpha_f - \alpha_r - \delta_f + \delta_r)$$
$$- \frac{l_r}{vI_z} \cdot (l_f F_{yf} - l_r F_{yr} + M_z) - \dot{\delta}_r \tag{8}$$

Here, α of two front/rear tyres are equal to each other, and δ_f of two front tyres are equal to each other. To achieve good control performance, the reference model has be established [19, 20].

2.3 Actuator fault model

Generally, the DDEV has to face different fault status caused by various actuator faults [22]. The two most common types of actuator faults, i.e. loss-of-effectiveness fault and the fault makes an actuator's control effect stuck at fixed level, are studied for the steering system and driving system of DDEV. The actuator fault is modelled in a generalized way as:

$$u_s = \sigma_s \cdot u_{ds} + \triangle u_s, s = 1, 2, 3, 4, 5, 6 \tag{9}$$

For the normal operating mode, $\sigma_s = 1$ and $\triangle u_s = 0$. If steering system gets stuck at a fixed level, $\sigma_p = c, p = 1, 2$ with c being a constant; thus, $0 < \sigma_p < 1$ and $\triangle u_p = 0$. For the steering system loss-of-effectiveness fault, $\triangle u_p = 0$ is defined and the parameter σ_p satisfies $0 < \sigma_p < 1$. The definition of faulty in-wheel motor is the same as the faulty steering system. When the stuck at a fixed-level fault occurs to in-wheel motor, the torque of the faulty in-wheel motor can be written as $T = T_d + \triangle T$ with T_d being the desired motor torque of the faulty motor and $\triangle T$ being the stuck torque. When a loss-of-effectiveness fault occurs to in-wheel motor, $T = \sigma_q \cdot T_d$ is defined with $0 < \sigma_q < 1, q = 3, 4, 5, 6$.

2.4 Control problem formulation

The analysis of the stability of DDEV is summed up as two problems:

(1) Different kinds of fault status problem. Each kind of fault status of DDEV may include different kinds of actuator faults, including the loss-of-effectiveness fault and struck at a fixed-level fault. However, the type of faults status is usually uncertain, and the fault-tolerant controller should be designed independently for different actuator faults to guarantee the stability of DDEV [23]. Besides, the normal status of DDEV should be considered in this analysis. Therefore, the stability control problem can be summarized as the various fault status problem, and the fault-tolerant problem needs to be investigated based on multiple model method [24].

(2) Switching problem between various operating status. The DDEV usually works under various operating status, including normal and fault status. Conventional stability control strategies cannot achieve stable switching between different operating status [25]. The direct switching between various operating status is also unstable.

3 The multiple model-based fault-tolerant control system

The proposed MMFTCS includes an operating status recognizer and a fault-tolerant controller set, and its structure is shown in Fig. 2, the operating status recognizer is designed to distinguish normal or fault status using fuzzy logic, the fault-tolerant controller set is proposed to achieve optimal fault-tolerant control and smooth switching, and the robustness analysis of the MMFTCS is presented. The advantages of MMFTCS are presented as:

(1) To distinguish normal or fault status accurately, a fuzzy logic strategy is designed to realize model matching, with the characteristic of being suitable for solving the problem of nonlinear and various variables, in the operating status recognizer.

(2) To solve the multiple constrained optimal control problem of the various actuator faults, a novel LQR-MPC is designed for this complex and fast sampling system, in the fault-tolerant controller set.

(3) To guarantee the practicability to each typical operating mode, and to achieve smooth switching, the output of MMFTCS is computed by the weighted signal of each LQR-MPC, using the weight coefficient.

3.1 Design of the operating status recognizer

To distinguish normal or fault status accurately, the operating status recognizer is designed based on multiple model method. (1) In Sect. 3.1.1, the operating status of DDEV is analyzed and summarized as eight typical operating modes, including a normal mode and seven fault modes. A typical operating mode set is established to describe the characteristic of the corresponding typical operating mode accurately. (2) In Sect. 3.1.2, the matching degree between current operating status and typical operating mode set is analyzed and represented as the weight coefficient and calculated by fuzzy logic.

3.1.1 The establishment of typical operating mode set

The offline typical operating mode set is established for evaluating the characteristic of DDEV. The main merits of
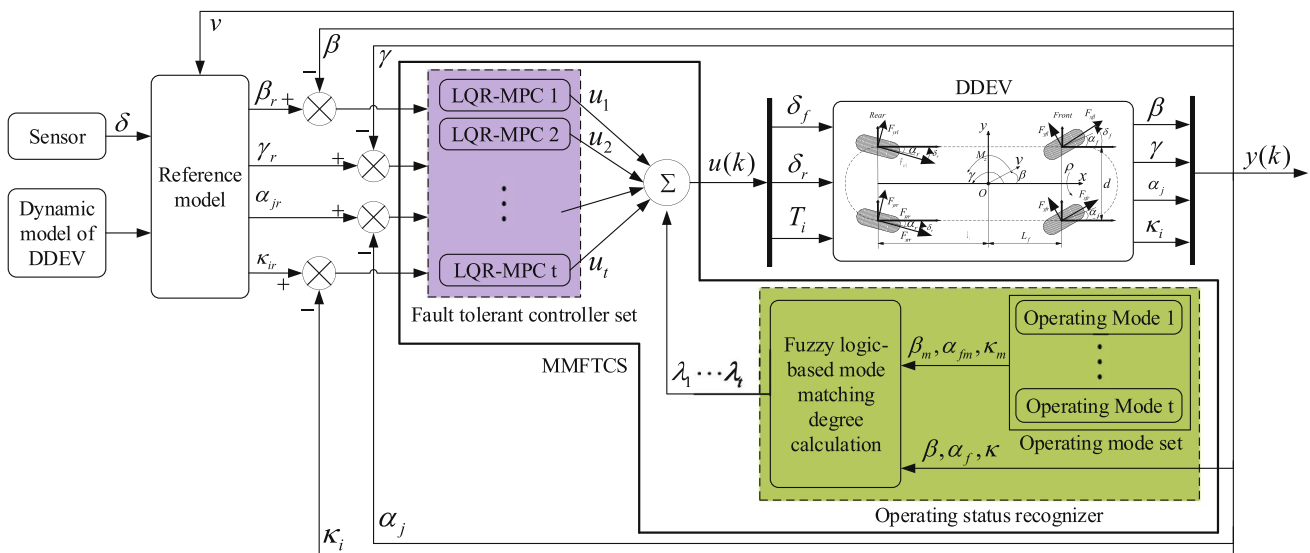

Fig. 2 The structure of the MMFTCS for DDEV

the selected variables β, α_f and κ_{fl} include: (1) they both have significant differences under different operating status; (2) the error between the actual value and reference model varies within a fixed interval under one special operating status; (3) they can represent the yaw, lateral and longitudinal stability of DDEV comprehensively.

The steps of the establishment of typical operating mode set are shown as:

Step 1 Obtain the parameters of various operating status.

Under different operating status, σ_s and $\triangle u_s$, $s = 1, 2, 3, 4, 5, 6$ are different. The parameters of various fault status are set according to experiences as shown in Table 2. The possible combinations of the actuator faults are calculated as $2^3 = 8$, and the number of the normal status is 1. When a loss of-effectiveness fault occurs to steering system, $\sigma_p = 5$, $p = 1, 2$ and $\triangle u_p = 0$.

Step 2 Test the performance of various fault status.

The simulations are carried to investigate the performance under specific fault status. Obviously, β, α_f and κ_{fl} can represent the yaw, lateral and longitudinal stability of DDEV, respectively. As shown in Fig. 3, the values of β, α_f and κ_{fl} have significant differences under different operating status. The error $\triangle\beta$ between actual β and reference model β_r varies within fixed interval under one special operating status, and $\triangle\alpha_f$ and κ_{fl} are the same. Therefore, various operating status can be represented by $\triangle\beta$, $\triangle\alpha_f$ and κ_{fl}.

Step 3 Obtain the classification of typical operating modes.

The performance of eight typical operating modes is shown in Table 3. Also, the characteristics of the steering system struck at a fixed level and driving system normal operating mode and the steering system struck at a fixed level and driving system loss-of-effectiveness operating mode are very similar. The details of this phenomenon are

explained in Fig. 4. Thus, the number of fault mode is seven and the number of normal mode is one.

3.1.2 The fuzzy logic-based model matching

The fuzzy logic strategy is applied to weight coefficient calculation and beneficial to the practical application for the proposed MMFTCS [26].

The input variables of fuzzy logic are actual operating status $[\triangle\beta, \triangle\alpha_f, \kappa_{fl}]^T$ and typical operating mode $[\triangle\beta_m, \triangle\alpha_{fm}, \kappa_{flm}]^T$. The output variables are membership values θ_t, $t = 1, 2, 3, 4, 5, 6, 7, 8$. Fuzzy inference technique via Mamdani method is adopted due to its simple structure [27]. The membership functions for $\triangle\beta$, $\triangle\alpha_f$ and κ_{fl} are set, as shown in Fig. 5. $\triangle\beta$ is divided into three levels in Fig. 5a: small (S), medium (M) and big (B). $\triangle\alpha_f$ is divided into five levels in Fig. 5b: very small (VS), small (S), medium (M), big (B) and very big (VB). κ_{fl} is divided into two levels in Fig. 5c: medium (M) and big (B). The membership value θ is divided into eight levels in Fig. 5d: very small (VS), medium small (MS), small (S), medium (M), big (B), medium big (MB), very big (VB) and super big (SB). The membership functions

Table 3 The performance of eight typical operating modes

Mode name	Value of $\triangle\beta$	Value of $\triangle\alpha_f$	Value of κ_{fl}
Operating mode 1	[0,0.0027)	[0.0043,0.0078)	[0.1,0.2]
Operating mode 2	[0,0.0027)	(0,0.0043)	[0,0.1)
Operating mode 3	[0.0027,0.0059)	(0,0.0043)	[0.1,0.2]
Operating mode 4	[0.0027,0.0059)	=0	[0,0.1)
Operating mode 5	[0.0059,0.0123]	[0.0043,0.0067)	[0,0.1)
Operating mode 6	[0.0059,0.0123]	[0.0078,0.0113)	[0.1,0.2]
Operating mode 7	[0.0027,0.0059)	(0,0.0043)	[0,0.1)
Operating mode 8	[0,0.0027)	=0	[0,0.1)

Table 2 The parameters of various kinds of operating status

| Mode name	Operating status type	Value of σ_p	Value of σ_q	Value of $\triangle u_p$	Value of $\triangle u_q$
Operating mode 1	Steering system normal and in-wheel motor loss of effectiveness	1	10	0	0
Operating mode 2	In-wheel motor normal and steering system loss of effectiveness	5	1	0	0
Operating mode 3	Steering system loss of effectiveness and in-wheel motor loss of effectiveness	5	10	0	0
Operating mode 4	Steering system normal and in-wheel motor struck at a fixed level	1	1	0	$300 \times \cos(\frac{\pi}{30})$
Operating mode 5	Steering system struck at a fixed level and in-wheel motor normal	1	1	$\cos(\frac{\pi}{30})$	0
Operating mode 5	Steering system struck at a fixed level and in-wheel motor loss of effectiveness	1	10	$\cos(\frac{\pi}{30})$	0
Operating mode 6	Steering system loss of effectiveness and in-wheel motor struck at a fixed level	5	1	0	$300 \times \cos(\frac{\pi}{30})$
Operating mode 7	Steering system struck at a fixed level and in-wheel motor struck at a fixed level	1	1	$\cos(\frac{\pi}{30})$	$300 \times \cos(\frac{\pi}{30})$
Operating mode 8	Normal operating mode	1	1	0	0

(a) Performance of β

(b) Performance of α_f

(c) Performance of κ_{fl}
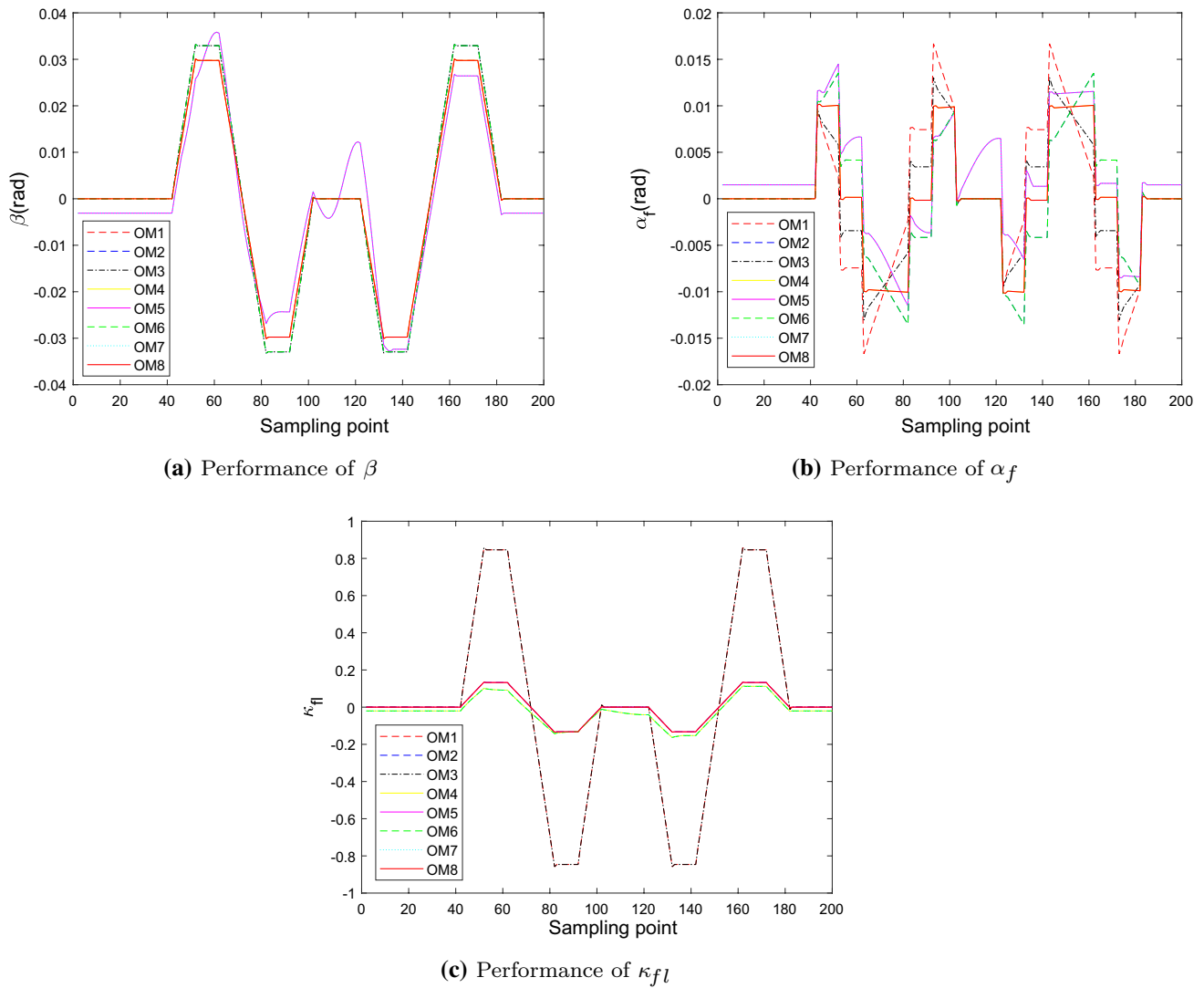
Fig. 3 The tests under eight typical operating modes

of the eight membership values $\theta_t, t = 1, 2, 3, 4, 5, 6, 7, 8$ are identical. Table 4 shows the rule set in the fuzzy inference system (FIS). The rule set includes $2 \times 3 \times 5 = 30$ rules.

Normalization is carried out to calculate the weight coefficients λ_t, where $t = 1, 2, 3, 4, 5, 6, 7, 8$ represent eight typical operating modes. Here, $\sum_{t=1}^{t=8} \lambda_t = 1$ and $\lambda_t \in [0, 1]$.

$$\lambda_t = \frac{\theta_t}{\sum_{t=1}^{t=8} \theta_t} \qquad (10)$$

where θ_t is membership value of eight typical operating modes.

3.2 Design of the fault-tolerant controller set

To deal with the stability problem in the operating status detected by the operating status recognizer, and to

achieve smooth switching, the fault-tolerant controller set is designed.

3.2.1 The discrete state-space model and objective functions

The method of solving the stability problem is to tune the values of β, γ, α_f, α_r and κ within the stable range. In the discrete state-space model, the state variables are defined as $x = [\beta, \gamma, \alpha_f, \alpha_r, \kappa_{fl}, \kappa_{fr}, \kappa_{rl}, \kappa_{rr}]^T$, and the control variables are defined as $u = [\delta_f, \delta_r, T_{fl}, T_{fr}, T_{rl}, T_{rr}]^T$.

$$x(k + m \mid k) = f^k(x(k + m - 1 \mid k), u(k + m - 1 \mid k)) \cdot T_s \\ + x(k + m - 1 \mid k), 0 \leq m \leq \xi - 1 \qquad (11)$$

Then, the discretization of state-space model is defined as:

(a) Performance of β

(b) Performance of α_f

(c) Performance of κ_{fl}
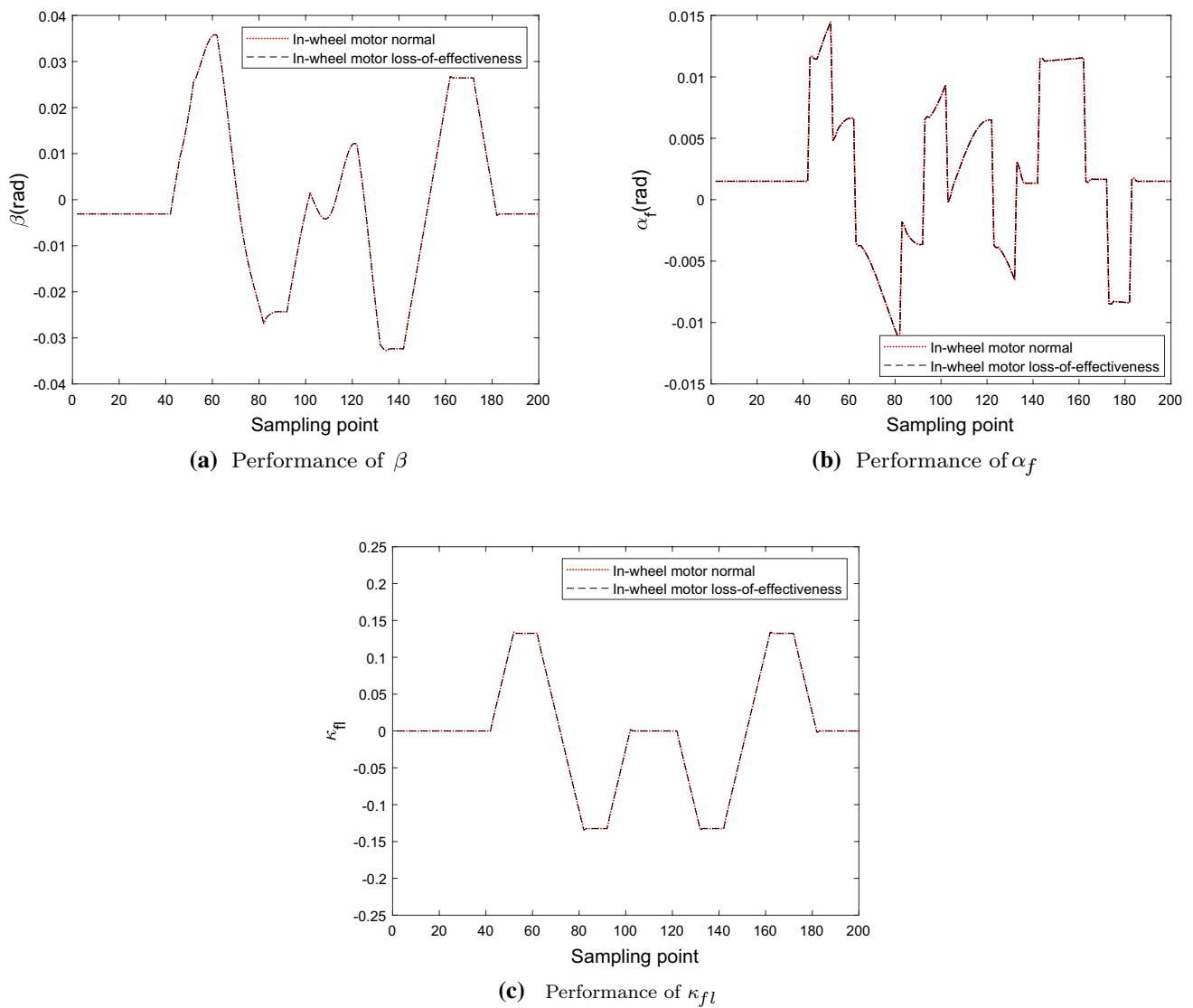
Fig. 4 The tests under steering system struck at a fixed level and in-wheel motor normal/loss of effectiveness

$$x_1(k+1) = T_s \cdot \frac{F_{yf}(x_1(k), x_2(k), u_1(k))}{mv} + x_1(k) + T_s \cdot \frac{F_{yr}(x_1(k), x_2(k), u_2(k))}{mv} \tag{12}$$

$$x_2(k+1) = T_s \cdot \frac{l_f \cdot F_{yf}(x_1(k), x_2(k), u_1(k))}{I_z} - T_s \cdot \frac{l_r \cdot F_{yr}(x_1(k), x_2(k), u_2(k))}{I_z} + T_s \cdot \frac{M_z}{I_z} + x_2(k) \tag{13}$$

$$x_3(k+1) = T_s \cdot \frac{F_{yf}(x_1(k), x_2(k), u_1(k))}{mv} + x_3(k) + T_s \cdot \frac{F_{yr}(x_1(k), x_2(k), u_2(k))}{mv} - \frac{T_s \cdot v}{l_f + l_r} \cdot (x_3(k) - x_4(k) - u_1(k) + u_2(k)) - \dot{u}_1(k) + \frac{T_s \cdot l_f}{vI_z} \cdot (l_f F_{yf} - l_r F_{yr} + \frac{u_3(k) + u_4(k) + u_5(k) + u_6(k)}{r}) \tag{14}$$

Table 4 The fuzz logic rule set

κ_{fl}	$\triangle\alpha_f$	$\triangle\beta$	θ_1	θ_2	θ_3	θ_4	θ_5	θ_6	θ_7	θ_8
M	S	VS	S	VB	M	SB	B	MS	MB	VS
M	S	S	S	SB	M	MB	B	MS	VB	VS
M	S	M	S	MB	MS	B	SB	M	VB	VS
M	S	B	S	MB	MS	B	SB	M	VB	VS
M	S	VB	S	MB	MS	B	SB	M	VB	VS
M	M	VS	S	VB	M	SB	B	MS	MB	VS
M	M	S	M	VB	S	B	MB	MS	SB	VS
M	M	M	S	MB	MS	B	SB	M	VB	VS
M	M	B	S	MB	MS	B	SB	M	VB	VS
M	M	VB	S	MB	MS	B	SB	M	VB	VS
M	B	VS	S	MB	MS	B	SB	M	VB	VS
M	B	S	S	MB	MS	B	SB	M	VB	VS
M	B	M	S	MB	MS	B	SB	M	VB	VS
M	B	B	S	MB	MS	B	SB	M	VB	VS
M	B	VB	S	MB	MS	B	SB	M	VB	VS
B	S	VS	VB	B	SB	S	MS	MB	M	VS
B	S	S	SB	B	VB	M	MS	MB	S	VS
B	S	M	SB	B	VB	M	MS	MB	S	VS
B	S	B	SB	B	VB	M	MS	MB	S	VS
B	S	VB	VB	S	MB	MS	B	SB	M	VS
B	M	VS	VB	B	SB	S	MS	MB	M	VS
B	M	S	VB	B	SB	S	MS	MB	M	VS
B	M	M	SB	B	VB	M	MS	MB	S	VS
B	M	B	SB	B	VB	M	MS	MB	S	VS
B	M	VB	VB	S	MB	MS	B	SB	M	VS
B	B	VS	VB	S	MB	MS	B	SB	M	VS
B	B	S	VB	S	MB	MS	B	SB	M	VS
B	B	M	VB	S	MB	MS	B	SB	M	VS
B	B	B	VB	S	MB	MS	B	SB	M	VS
B	B	VB	VB	S	MB	MS	B	SB	M	VS

$$x_4(k+1) = T_s \cdot \frac{F_{yf}(x_1(k), x_2(k), u_1(k))}{mv} + x_4(k) + T_s \cdot$$
$$\frac{F_{yr}(x_1(k), x_2(k), u_2(k))}{mv}$$
$$- \frac{T_s \cdot v}{l_f + l_r} \cdot (x_3(k) - x_4(k) - u_1(k) + u_2(k)) \quad (15)$$
$$- \dot{u}_2(k) - \frac{T_s \cdot l_r}{vI_z} \cdot (l_f F_{yf}$$
$$- l_r F_{yr} + \frac{u_3(k) + u_4(k) + u_5(k) + u_6(k)}{r})$$

$$x_n(k+1) = \left(\left(\frac{4 \cdot (x_n(k)+1)}{m \cdot v} + \frac{(x_n(k)+1)^2 \cdot r^2}{J \cdot v}\right) \cdot$$
$$C_n \cdot T_s + 1\right) \cdot x_n(k) \quad (16)$$
$$- \frac{(x_n(k)+1)^2 \cdot r \cdot T_s}{J \cdot v} \cdot u_{n-2}(k), n = 5, 6, 7, 8$$

To solve the optimal control problem, the objective function of the LQR-MPC J_{mpc} is formulated based on discrete form, as shown in three parts as: (a) To make β, γ, α_f, α_r and κ track the required reference model quickly as: $J_1 = \parallel x(k) - R_r(k) \parallel_Q^2$, where Q plays regulatory role in tracking the expectations to maintain vehicle stable. R_r denotes the reference model. (b) To compensate the feedback error $e(k) = y(k) - R_r(k)$ as: $J_2 = \parallel y(k) - R_r(k) \parallel_R^2$, where R is weight matrix to minimizing the feedback error. (c) To enforce the control variables within the stable range as: $J_3 = \parallel u(k) \parallel_F^2$.

$$J_{mpc}(x(k), u(k)) = J_1 + J_2 + J_3 = \parallel x(k) - R_r(k) \parallel_Q^2$$
$$+ \parallel y(k) - R_r(k) \parallel_R^2 + \parallel u(k) \parallel_F^2 \quad (17)$$

3.2.2 The design of LQR-MPC

A total of eight LQR-MPCs are designed for these typical operating modes, including a normal mode and seven fault

(a) Membership function of $\triangle \beta$

(b) Membership function of $\triangle \alpha_f$

(c) Membership function of κ_{fl}

(d) Membership function of θ
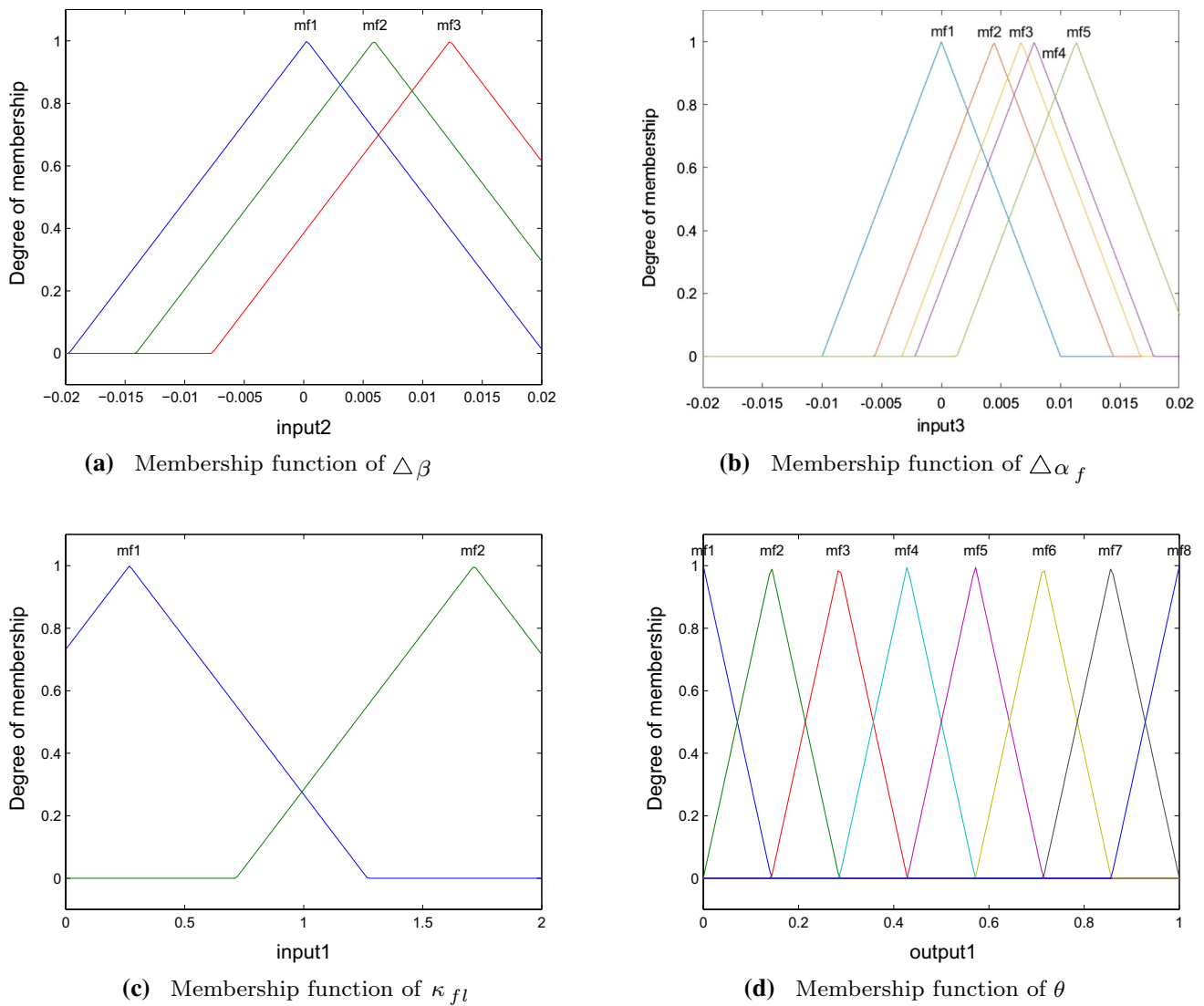
Fig. 5 The membership functions

modes. The designed LQR-MPC is implemented as [28–30]: The LQR method is applied to deal with the loss-of-effectiveness fault σ and to obtain optimal control variables. The MPC-based observer is designed to deal with the struck at a fixed-level fault $\triangle u(k)$.

To obtain the optimal control variables $u(k)$, the state feedback law is adopted [31], and the LQR is adopted to obtain the state feedback matrix K. At time instant k, the state feedback law is as:

$$u(k) = K \cdot x(k) \tag{18}$$

where the optimal state variable $x(k)$ is obtained by solving $min \frac{1}{2} x^T H x + f^T x$. The objective function of the LQR is designed as $\dot{x}^T P \dot{x} + x^T P x + x^T K^T R K\, x + x^T Q x = 0$, where $K = R^{-1}(B\sigma)^T P$ and σ is incorporated, and thus σ can be tolerated in the LQR-MPC.

To estimate $\triangle u(k)$, an MPC-based observer is proposed in the LQR-MPC. The estimation capacity of MPC can be

Fig. 6 The 8DOF vehicle model

Table 5 Test environment setting

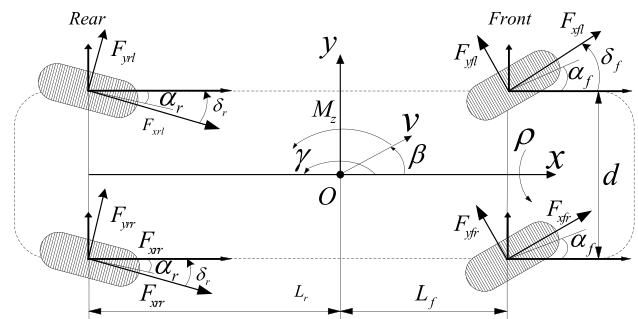| Name	Test 1	Test 2
Manoeuvre	Five operating status	Seven operating status
Initial speed	20 km/h	20 km/h
Acceleration	0.4125 m/s	0.4125 m/s
μ	0.6	0.6
Switching point	60, 100, 120, 165	75, 135, 160, 215, 245, 300
Actuator fault on motor torque	$cos(\frac{\pi}{30} \cdot k) + 300$ Nm, $\sigma = 10$	$cos(\frac{\pi}{30} \cdot k) + 300$ Nm, $\sigma = 10$
Actuator fault on steering angle	$cos(\frac{\pi}{30} \cdot k) + 0.3$ rad, $\sigma = 5$	$cos(\frac{\pi}{30} \cdot k) + 0.3$ rad, $\sigma = 5$
Stable range of γ	$[-0.3, 0.3]$ rad/s	$[-0.3, 0.3]$ rad/s
Stable range of α_f	$[-0.02, 0.02]$ rad	$[-0.02, 0.02]$ rad
Stable range of κ	$[-0.02, 0.02]$	$[-0.02, 0.02]$
Stable range of T	$[-2000, 2000]$ Nm	$[-2000, 2000]$ Nm

utilized for fault estimation [32]. The system (12–16) can be reformulated as:

$$\hat{x}(k + 1) = A \cdot \hat{x}(k) + B \cdot \sigma(k) \cdot u_d(k) + B \cdot \triangle u(k) \qquad (19)$$

$$\hat{y}(k) = C \cdot \hat{x}(k) \qquad (20)$$

where $\hat{y}(k)$ is the estimated output when actuator fault is considered. The $\hat{x}(k)$ is acquired by using (20) recursively. The error between the estimated output $\hat{y}(k)$ and the actual output of $y(k)$ can be used by the MPC-based observer to estimate $\triangle u(k)$. Therefore, minimization of the objective function is reformulated into the optimization problem: $J_{obs}(x(k), u_{obs}(k)) = \| \hat{y}(k) - y(k) \|_S^2$, where the weighted matric S is chosen as a matrix with suitable dimensions. The observer input $u_{obs}(k)$ is obtained and $u_{obs}(k) = \sigma(k) \cdot u_d(k) + \hat{\triangle} u(k)$. Here, $\sigma(k)$ is set to be 1, which means that the loss-of-effectiveness fault is ignored. $\hat{\triangle}u(k)$ can be estimated as:

$$\hat{\triangle}u(k) = u_{obs}(k) - u_d(k) \qquad (21)$$

where $u_d(k)$ is obtained by $x(k)$ as previously described. In this way, $\hat{\triangle}u(k)$ can be estimated, and $\triangle u(k)$ can be tolerated effectively.

In the LQR-MPC, the optimal command signal is applied to the process only during the following sampling interval:

$$y(k + m \mid k) = C \cdot f^k(x(k + m - 1 \mid k), u(k + m - 1 \mid k)) \cdot T_s \\ + C \cdot x(k + m - 1 \mid k), 1 \le m \le \rho \qquad (22)$$

where ρ is defined as predictive horizon and $\xi = \rho = 2$.

3.2.3 Weighed output of the MMFTCS

To solve the problem of guaranteeing the practicability to each typical operating mode, and to achieve smooth switching, the weighting method is adopted in the MMFTCS [25].

At each sampling time k, the weight coefficients of current operating status $\lambda_t(k)$, and the optimal outputs of the fault-tolerant controller $u_t(k)$ have been calculated, where $t = 1, 2, 3, 4, 5, 6, 7, 8$ represent eight typical operating modes. In addition, the output of each LQR-MPC is the discrete value. The weighted outputs of LQR-MPC constitute the control output of MMFTCS as:

$$u(k) = \sum_t^{t=8} \lambda_t \cdot u_t(k), t = 1, 2, 3, 4, 5, 6, 7, 8 \qquad (23)$$

where $u_t(k)$ is optimal control output calculated by LQR-MPC of tth typical operating mode and λ_t is the weight coefficient of tth typical operating mode.

3.3 Robustness analysis of MMFTCS

Considering the following function, it is assumed that $V(x) > 0$ as:

$$V(x) = x^T \phi x > 0 \qquad (24)$$

As $u = -(R^{-1}B^T \phi)x$ is assumed, a positive definite matrix ϕ is assumed to satisfy: $\frac{d(x^T \phi x)}{dt} = -x^T(Q + (R^{-1}B^T \phi)^T R(R^{-1}B^T \phi))x$. Then, it is expanded as the Riccati function (25):

$$(A - B(R^{-1}B^T \phi))^T \phi + \phi(A - B(R^{-1}B^T \phi)) \\ + (R^{-1}B^T \phi)^T R(R^{-1}B^T \phi) + Q = 0 \qquad (25)$$

where Q and R are weight matrices in the objective function (17).

As matrices Q, B and R are known. When matrix ϕ satisfies (24) and (25) simultaneously, it is proved to be satisfied as:

(a) Weight coefficient λ

(b) Vehicle yaw rate γ

(c) Front wheel side slip angle α_f

(d) Rear wheel side slip angle α_r

(e) Distribution of longitudinal slip ratio κ

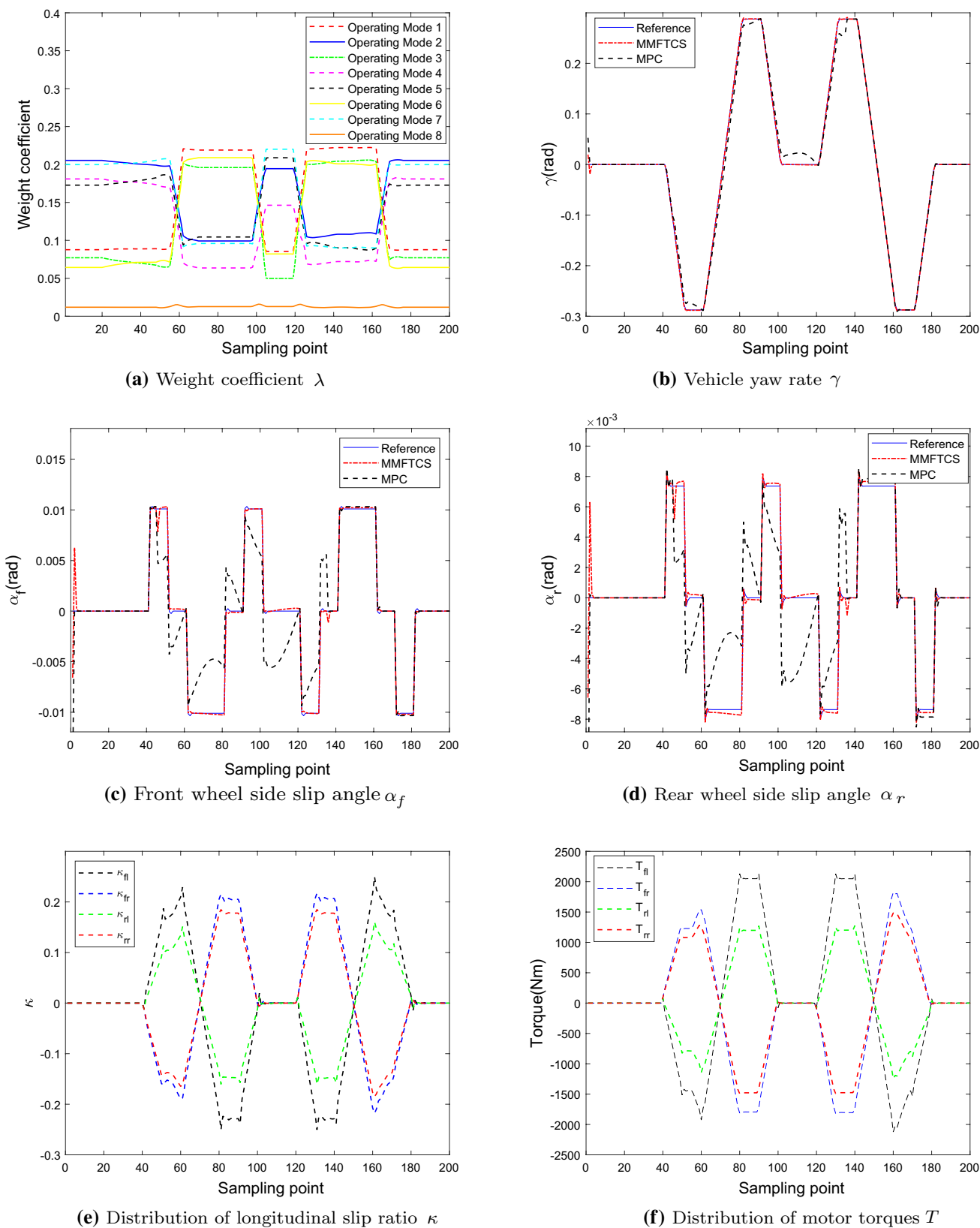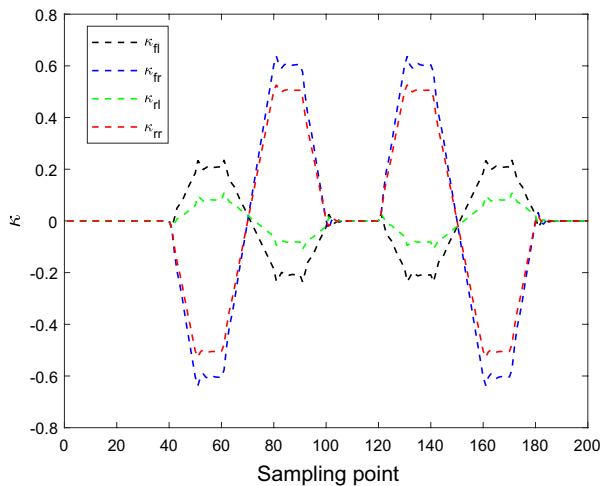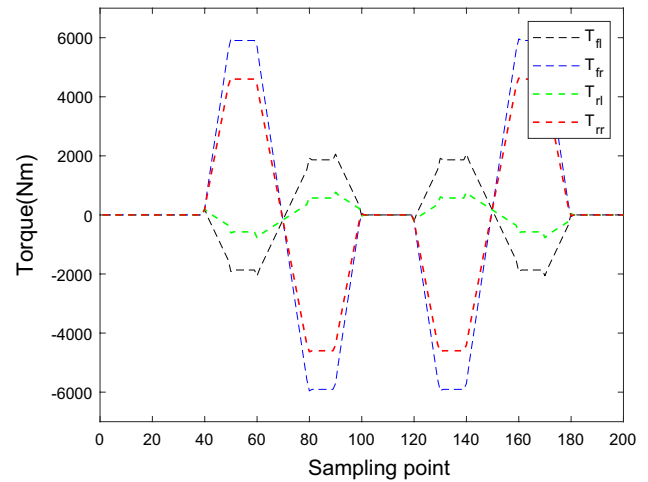**(f)** Distribution of motor torques T

Fig. 7 The stability performance of DDEV by the MMFTCS under Test 1

(a) Distribution of longitudinal slip ratio κ

(b) Distribution of motor torques T

Fig. 8 The stability performance of DDEV by the MPC under Test 1

$$\frac{\mathrm{d}(x^T \phi x)}{\mathrm{d}t} = -x^T (Q + (R^{-1}B^T\phi)^T R(R^{-1}B^T\phi))x < 0 \qquad (26)$$

As a result, the Lyapunov function can be solved and matrix ϕ is adopted at the state of the control horizon. In the experiment, the values of matric ϕ can be obtained over the sampling horizon. Therefore, the robustness of the MMFTCS is guaranteed.

4 Simulation comparison and analysis

To verify the performance of the proposed MMFTCS, comprehensive simulation under MATLAB environment is conducted. The simulation is evaluated on an

The values of parameters in vehicle model are set in Table 1.

(2) Parameter setting of the MMFTCS

The values of parameters in the MMFTCS are set as: $T_s = 5 \times 10^{-2}$, $Q = 10^4 \times \mathrm{diag}(1, 1, 1, 1, 1, 1, 1, 1)$, $R = 10 \times \mathrm{diag}(1, 1, 1, 1, 1, 1, 1, 1)$, $S = 10 \times \mathrm{diag}(1, 1, 1, 1, 1, 1, 1, 1)$, $F = 10 \times \mathrm{diag}(1, 1, 1, 1, 1)$. $C = \mathrm{diag}(1 : 1 : 1 : 1 : 1 : 1 : 1 : 1)$. ϕ is varied because of the various kinds of operating status. For example, the ϕ at sampling point 100 is shown as (27).

$$\phi = \begin{bmatrix} -1.1142 & 0.2038 & -3.3252 & 4.3199 & -0.0235 & 0.0235 & -0.0234 & 0.0234 \\ -1.2607 & 0.2328 & -0.1264 & 0.02079 & -0.0109 & 0.0109 & -0.0108 & 0.0108 \\ 0.8420 & -0.1637 & 1.9990 & -2.5480 & 0.0158 & -0.0159 & 0.0158 & -0.0158 \\ -1.1045 & 0.2147 & -2.5480 & 3.2645 & -0.0205 & 0.0205 & -0.0204 & 0.0204 \\ -0.0230 & 0.0045 & -0.0434 & 0.0561 & -4284 & 3856 & 3839 & 3840 \\ 0.0230 & -0.0045 & 0.0434 & -0.0561 & 3856 & -4329 & 3840 & 3840 \\ -0.0229 & 0.0044 & -0.0432 & 0.0559 & -3839 & 3840 & -2853 & 3824 \\ 0.0229 & -0.0044 & 0.0432 & -0.0559 & 3840 & 3840 & 3824 & 2880 \end{bmatrix} \qquad (27)$$

eight-degrees-of-freedom (8DOF) simulation platform, as shown in Fig. 6.

4.1 Parameter and test environment settings

(1) Parameter setting of vehicle model

(3) Test environment setting

In this work, two typical tests are carried out in Table 5. The results are compared with the performance of one general MPC, which means that only one model predictive controller is adopted to realize stable steering of vehicle [16]. The stable range of DDEV is obtained by the constraints of vehicle.

(a) Weight coefficient λ

(b) Vehicle yaw rate γ

(c) Front wheel side slip angle α_f

(d) Rear wheel side slip angle α_r

(e) Distribution of longitudinal slip ratio κ

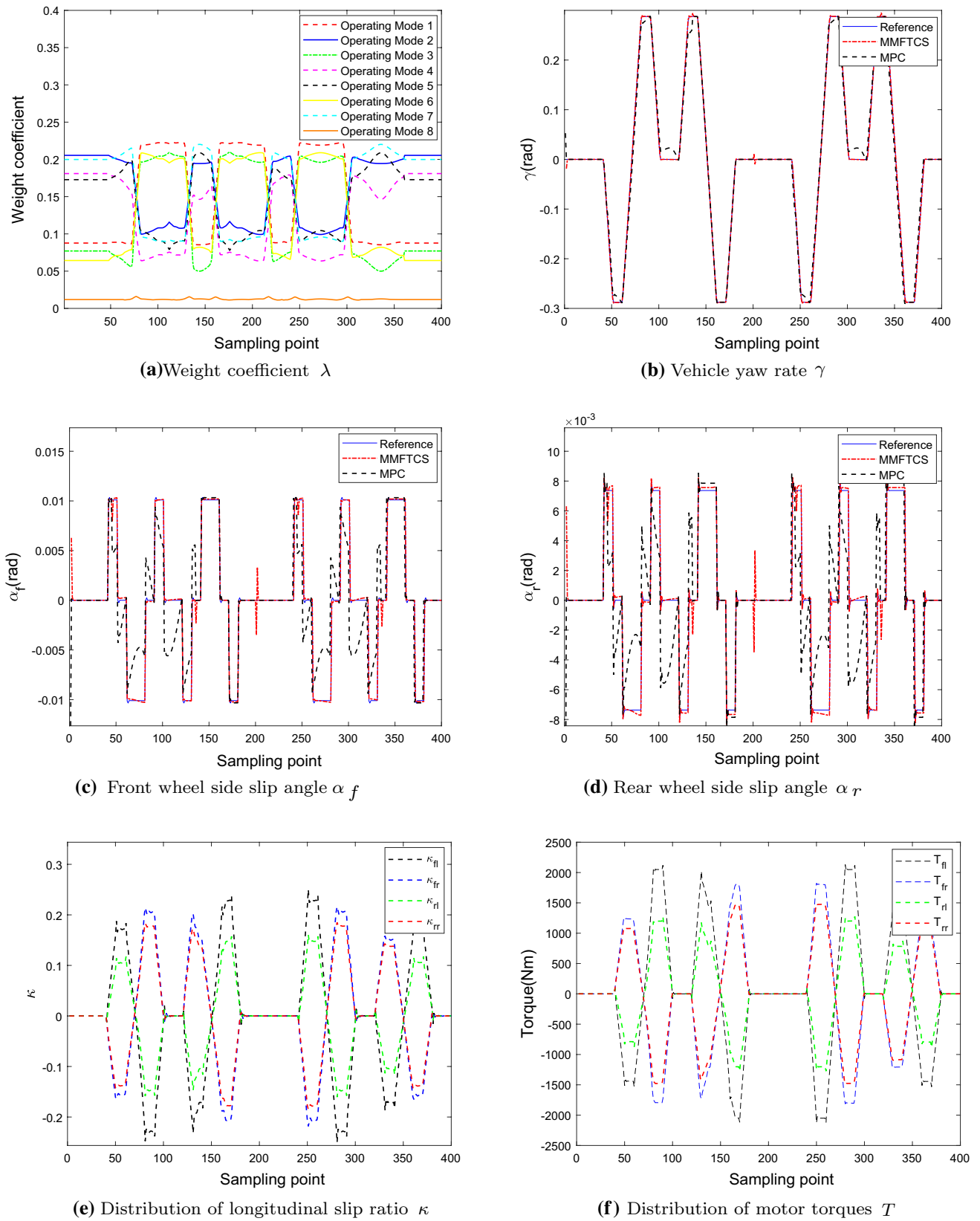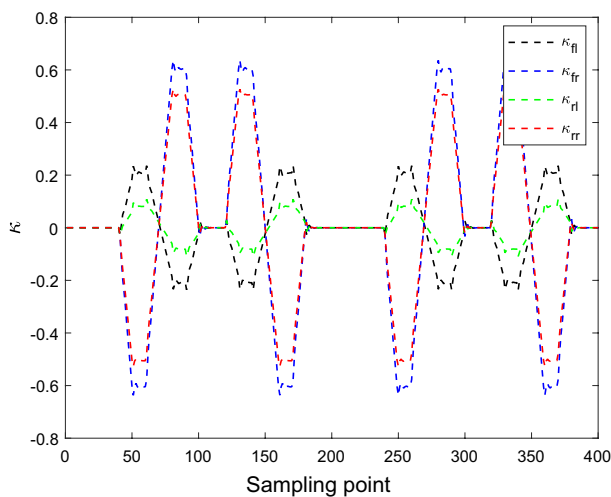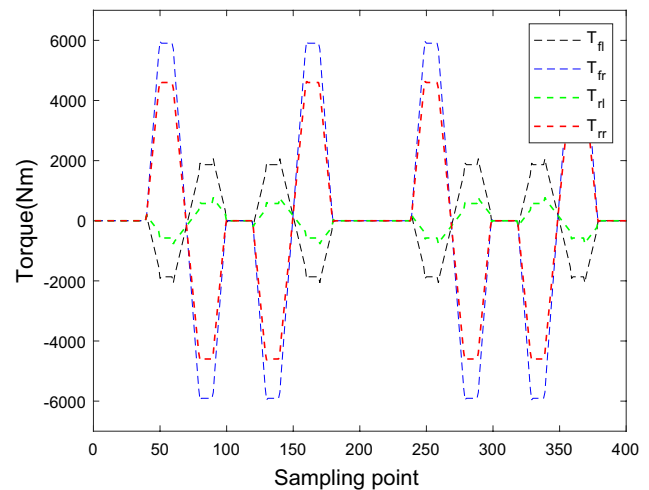**(f)** Distribution of motor torques T

Fig. 9 The stability performance of DDEV by the MMFTCS under Test 2

(a) Distribution of longitudinal slip ratio κ **(b)** Distribution of motor torques T

Fig. 10 The stability performance of DDEV by the MPC under Test 2

4.2 Test 1

The simulation results under Test 1 are shown in Figs. 7 and 8.

By the MMFTCS, the values of $\lambda_t(k)$ which can represent each kind of operating status are changed correspondingly with the switching of the operating status. γ tracks reference curve well with the error less than 0.002 rad/s. α_f and α_r are kept within the stable range. α_f tracks reference model well with the error less than 0.005 rad. The curve of α_r is close to the reference model. The switching performance of α_f and α_r between operating status is stable. κ is constrained in the stable range. T is constrained in the stable range. T at the right tyres is larger than that at the left tyres when the vehicle turns left. The reason is that the tyre yaw moment is generated from tyre yaw motion.

By the MPC, the maximum tracking error of γ is about 0.05 rad/s. The maximum tracking error of α_f is about 0.015 rad. The switching performance of α_f and α_r is instable at sampling points 60, 100 and 120. The performance of κ and T is over the stable ranges. As previously described, the five kinds of operating status are the same.

4.3 Test 2

The simulation results under Test 2 are shown in Figs. 9 and 10.

By the MMFTCS, $\lambda_t(k)$ can represent each kind of operating status accurately. γ is kept within the stable range with the error less than 0.001 rad/s. Also, the switching performance of γ between operating status is smooth, with less

oscillatory behaviour. α_f tracks reference model well with the error less than 0.002 rad. Both α_f and α_r are kept within the stable range. α_f and α_r change smoothly between operating status. κ is constrained in the stable range. It can be revealed that T is constrained in the stable range. T at the right tyres is larger than that at the left tyre when the vehicle turns left.

Conversely, by the MPC, the switching performance of γ is instable at sampling points 135 and 300. The maximum tracking error of α_f is about 0.015 rad. Additionally, the switching performance of α_f and α_r is instable at sampling points 135, 245 and 300. κ and T are over the stable ranges.

5 Conclusions

This paper proposes a novel MMFTCS to deal with various kinds of fault status problem. The robustness of the proposed MMFTCS has been verified. The simulation results show the fault-tolerant performance of the proposed control system. The MMFTCS can also accurately keep the vehicle within the stable range to ensure the stability of DDEV. Moreover, the switching performance between operating status is stable. As a result, the optimal fault-tolerant control and smooth switching performance under various kinds of operating status can be achieved by the MMFTCS efficiently.

References

1. Zhang X, Gohlich D, Li J (2017) Energy-efficient toque allocation design of traction and regenerative braking for distributed drive electric vehicles. IEEE Trans Veh Technol 67(1):285–295

2. Shi K, Yuan XF, Huang GM, Liu ZX (2019) Weighted multiple model control system for the stable steering performance of distributed drive electric vehicle. J Braz Soc Mech Sci 41(1):201

3. Shi K, Yuan XF, Huang GM, He Q (2018) MPC-based compensation control system for the yaw stability of distributed drive electric vehicle. Int J Syst Sci 49(8):1795–1808

4. Gao ZW (2015) Fault Estimation and fault tolerant control for discrete-time dynamic systems. IEEE Trans Ind Electron 62(6):38740–3884

5. Zhang G, Zhang H, Huang X (2016) Active fault-tolerant control for electric vehicles with independently driven rear in-wheel motors against certain actuator faults. IEEE Trans Control Syst Technol 24(5):1557–1572

6. Yu M, Wang D (2014) Model-Based health monitoring for a vehicle steering system With multiple faults of unknown types. IEEE Trans Ind Electron 61(7):3574–3586

7. Kim S, Huh K (2016) Fault-tolerant braking control with integerated EMBs and regenerative in-wheel motors. Int J Automot Technol 17(5):923–936

8. Wang R, Wang J (2012) Fault-tolerant control for electric ground vehicles with independently-actuated in-wheel motors. ASME Trans J Dyn Syst Meas Control 134(2):194–203

9. Zheng B, Anwar S (2008) Fault-tolerant control of the road wheel subsystem in a steer-by-wire system. Int J Veh Technol 2008:1–8

10. Jeon N, Lee H (2016) Integrated fault diagnosis algorithm for motor sensors of in-Wheel independent drive electric vehicles. Sensors 16(5):99–111

11. Zhang H, Wang J (2017) Active steering actuator fault detection for an automatically-steered electric ground vehicle. IEEE Trans Veh Technol 66(5):3685–3702

12. Zheng B, Altemare C (2005) Fault tolerant steer-by-wire road wheel control system. Proc Am Control Conf 1619–1624:

13. Jing H, Wang R, Chadli M, Hu C, Yan F (2015) Fault-tolerant control of four-wheel independently actuated electric vehicles with active steering systems. IFAC Pap OnLine 48(21):1165–1172

14. Xu F, Olaru S, Puig V, Ocampo-Martinez C, Niculescu S (2017) Sensor-fault tolerance using robust MPC with set-based state estimation and active fault isolation. Int J Robust Nonlin 27(8):1260–1283

15. Li B, Du H, Li W (2016) Fault-tolerant control of electric vehicles with in-wheel motors using actuator-grouping sliding mode controllers. Mech Syst Sig Process 72:462–485

16. Rui L, Benmoussa S, Touati Y, Merzouki R, Bouamama BO (2014) Integration of fault diagnosis and fault-tolerant control for health monitoring of a class of MIMO intelligent autonomous vehicles. IEEE Trans Veh Technol 63(1):30–39

17. Wang R, Wang J (2011) Fault-tolerant control with active fault diagnosis for four-wheel independently-driven electric ground vehicles. IEEE Trans Veh Technol 60(9):4276–4287

18. Gao MZ, Cai GP, Nan Y (2016) Robust adaptive fault-tolerant H control of reentry vehicle considering actuator and sensor faults based on trajectory optimization. Int J Syst Sci 14(1):198–210

19. Rajamani R (2006) Vehicle dynamics and control, mechanical engineering series, 1st edn. Springer, Berlin

20. Pacejka HB (2005) Tyre and vehicle dynamics.seconded.London. Elsevier, UK

21. Shi K, Yuan XF, Huang GM (2019) DLMPCS-based improved yaw stability control strategy for DDEV. IET Intel Transp Syst 13(9):1329–1339

22. Wang R, Wang J (2012) Fault-tolerant control for electric ground vehicles with independently-actuated in-wheel motors. J Dyn Syst Trans ASME 134(2):194–203

23. Abbaspour A, Aboutalebi P, Yen KK, Sargolzaei A (2017) Neural adaptive observer-based sensor and actuator fault detection in nonlinear systems: Application in UAV. ISA Trans 67:317–329

24. Shi K, Yuan XF, Liu L (2018) Model predictive controller-based multi-model control system for longitudinal stability of distributed drive electric vehicle. ISA Trans 72:44–55

25. Sun X, Yuan C (2017) Model predictive control of an air suspension system with damping multi-mode switching damper based on hybrid model. Mech Syst Sig Process 94:94–110

26. Azeem H, Yellasiri S, Jammala V (2019) A fuzzy logic based switching methodology for a cascaded H-bridge multilevel inverter. IEEE Trans Power Electron 34(10):9360–9364

27. Anand K, Elangovan S (2019) Modelling and multi-objective optimization of ultrasonic inserting parameters through fuzzy logic and genetic algorithm. J Braz Soc Mech Sci 41(4):188

28. Lee D, Hu J (2017) Local model predictive control for T-S fuzzy systems. IEEE Trans Cybern 47(9):2556–2567

29. Nguyen HT, Kim EK, Kim IP, Han HC, Jung JW (2018) Model predictive control with modulated optimal vector for a three-Phase inverter with an LC filter. IEEE Trans Power Electron 33(3):2690–2703

30. Zhang R, Lu R, Xue A, Gao F (2016) New minmax linear quadratic fault-tolerant tracking control for batch processes. IEEE Trans Autom Control 61(10):3045–3051

31. Tao J, Ma L, Zhu Y (2016) Improved control using extended non-minimal state space MPC and modified LQR for a kind of nonlinear systems. ISA Trans 65:319–326

32. Rao CV, Rawlings JB, Mayne DQ (2008) Constrained state estimation for nonlinear discrete-time systems: Stability and moving horizon approximations. IEEE Trans Autom Control 48(2):246–258